ELSEVIER

Contents lists available at ScienceDirect

Continental Shelf Research

journal homepage: www.elsevier.com/locate/csr





The transition of tidal Kelvin waves to hybrid Kelvin edge and internal waves in the global ocean

Harpreet Kaur ^{a,*}, Maarten C. Buijsman ^a, Alexander E. Yankovsky ^b, Chan-Hoo Jeon ^c, Alan J. Wallcraft ^d

- ^a University of Southern Mississippi, Mississippi, USA
- ^b University of South Carolina, South Carolina, USA
- ^c I.M. Systems Group at Environmental Modeling Center (NOAA/NWS/NCEP/EMC), College Park, MD, USA
- ^d Florida State University, Florida, USA

ARTICLE INFO

Keywords: Kelvin wave Celtic sea/Bay of Biscay Barotropic energy flux HYCOM Internal tide

ABSTRACT

In this study, we investigate the transition of semidiurnal Kelvin waves into Hybrid Kelvin-Edge (HKE) waves and associated generation of internal tides at widening shelves using theory, a realistic global baroclinic ocean model simulation, and quasi-realistic regional barotropic model simulations. Using the global model simulation, we identify several areas where a tidal HKE wave transition co-exists with internal wave generation. Of all areas considered, the Celtic Sea/Bay of Biscay shelf has the widest shelf and the strongest internal tide generation. We find that the global simulation agrees better with the theoretical Kelvin modes on the narrow than with the hybrid edge modes on the wide shelves. To help us understand the effect of complex, realistic bathymetry on the HKE wave transition, we perform quasi-realistic 1/25° barotropic simulations of the Celtic Sea/Bay of Biscay shelf areas. In these simulations, we gradually change the realistic bathymetry to a more idealized bathymetry. The idealized simulations show that the complex bathymetry steers the barotropic energy flux and causes standing wave patterns, which mask the HKE wave transition. Based on this analysis, we conclude that the HKE wave transition in the Celtic Sea/Bay of Biscay and other shelf areas in the global ocean is most likely masked by the effects of complex bathymetry and that offshelf baroclinic fluxes cannot be exclusively attributed to the HKE wave transition.

1. Introduction

This study discusses the transition of barotropic zero mode Kelvin waves to zero mode Hybrid Kelvin-Edge (HKE) waves at widening shelves and the associated internal tide generation. Tidal waves propagate as coastal Kelvin waves where the coastal shelf is narrow and their restoring force is gravity and Earth's rotation (Mysak, 1980; Zhang and Yankovsky, 2016). Whereas Edge waves propagate along wide shelves, and their restoring force is gravity (Munk et al., 1970; Huthnance, 1975; Zhang and Yankovsky, 2016). A significant amount of tidal energy (70%) is dissipated on the continental shelves, of which about 70% is due to M₂ tides (Egbert and Ray, 2003). Hence, we are focusing on semidiurnal M₂ tides in this study. In contrast, a significant fraction of internal tide dissipates in deep water, where they contribute to mixing (Waterhouse et al., 2014; MacKinnon et al., 2017) and maintaining the overturning circulation (Munk and Wunsch, 1998; Kunze, 2017).

It has been found from numerical experiments that when a zero mode semidiurnal Kelvin wave (the sea surface height (SSH) amplitude does not have zero crossings in the cross-shore direction) traveling on a continental shelf along the coastal boundary encounters an increase in shelf width, it can convert into an Edge or HKE mode (Munk et al., 1970). HKE modes present on wide shelves possess the properties of both Kelvin waves and Stokes Edge waves for a certain frequency range (Ke and Yankovsky, 2010). They resemble Kelvin wave modes at lower frequencies and Edge wave modes at higher frequencies (Yankovsky, 2009; Ivanov et al., 2018). At intermediate frequencies, the group velocity is close to zero (Yankovsky, 2009). In this event, the net energy propagation in the alongshore direction is reduced, which drives the energy flux in the cross-shore direction (Yankovsky and Zhang, 2017).

The interaction of barotropic tides with the shelf bathymetry causes alongslope flows that move the isotherms/isopycnals in the vertical direction (Gerkema and Zimmerman, 2008). Due to this interaction,

E-mail address: harpreet.kaur@usm.edu (H. Kaur).

^{*} Corresponding author.

barotropic tidal energy is converted to baroclinic tidal energy resulting in the generation of internal waves (Huthnance, 1981; Buijsman et al., 2020). One of the mechanisms that cause the generation of internal tides from barotropic tides is the HKE wave transition. Idealized numerical experiments have demonstrated that the conversion of M2 zero mode Kelvin waves to zero mode HKE waves can transmit a significant fraction (more than 10%) of barotropic energy into internal tides (Yankovsky and Zhang, 2017). Associated with this process is a barotropic energy flux circulation pattern, in which the net alongshore flux is almost reduced to zero due to the opposite directions of the alongshore fluxes on and off the shelf. An example of such a flux pattern on a widening shelf is shown in Fig. 1. In this flux pattern, the alongshore barotropic energy flux changes its direction towards the shore on the wide shelf causing the generation of offshelf baroclinic energy fluxes (Circulation A in Fig. 1) (Yankovsky and Zhang, 2017). An offshelf barotropic flux occurs at the upstream location of the wide shelf. These cross-shelf barotropic energy fluxes are not part of the modal wave structure but occur due to wave adjustment from one type of shelf topography to another. This pattern can coincide with a small anticlockwise flux pattern on the wide shelf (Circulation B in Fig. 1). The clockwise flux pattern is generally linked to the generation of internal waves as observed in idealized model simulations of Zhang and Yankovsky (2016) and Yankovsky and Zhang (2017). Examples of widening shelves that generate internal tides are Northwest Australia, Celtic Sea/Bay of Biscay (hereafter referred to as the CB shelf), Amazon, and Sierra Leone shelves (Buijsman et al., 2020).

In this study, we investigate the scattering process of M2 barotropic zero mode HKE waves at widening shelves using theory (Brink and Chapman, 1987), a realistic global baroclinic ocean model simulation, and quasi-realistic regional barotropic model simulations. We are focusing on zero coastal modes because propagating higher modes do not exist at the M2 frequency (Ke and Yankovsky, 2010). Moreover, We assume that the zero modes are fully barotropic. In reality, baroclinic and barotropic modes may not be clearly separated for coastal modes (Dale et al., 2001; Musgrave, 2019). Our first objective is to find areas in the global ocean where a transition from a zero mode Kelvin wave to a HKE wave mode may occur. Our second objective is to identify shelf areas where internal waves are generated due to the HKE wave conversion. For this purpose, we use the global baroclinic ocean simulation. Our third objective is to understand the effect of realistic bathymetry on the HKE wave transition. To achieve this, we perform regional barotropic model simulations in the CB area for bathymetry configurations ranging from realistic to idealized. The CB has a very wide shelf and a large offshelf baroclinic energy flux. We investigate if this flux is related to the HKE wave transition mechanism.

The rest of the paper is organized as follows: Section 2 explains the theory, model simulations, and the applied methodology. In section 3,

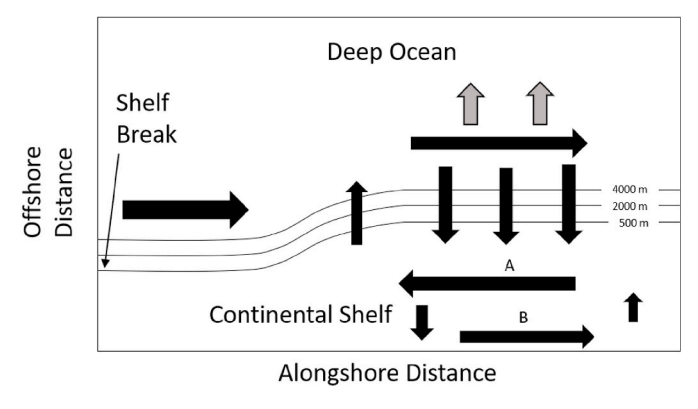


Fig. 1. Schematic of the M_2 barotropic and baroclinic flux circulation patterns due to the HKE wave transition on a widening shelf. Black (gray) arrows show the direction of the barotropic (baroclinic) energy flux.

we present the results from the global and regional analyses. We end with discussions and conclusions in section 4.

2. Models and methodology

In this section, we discuss the theory of the HKE wave mechanism and how we apply this theory to the global baroclinic and regional barotropic model simulations.

2.1. Theory

In the theory of Brink and Chapman (1987), the linear shallow water equations are used with the *f*-plane approximation for a non-viscous fluid of uniform density (Huthnance, 1975; Zhang and Yankovsky, 2016). The equation for this well-known boundary problem (Huthnance, 1975; Mysak, 1980), based on one-dimensional (1D) shelf geometry and linearized momentum equations, is:

$$\frac{d^2\eta}{dy^2} + \frac{1}{h}\frac{dh}{dy}\frac{d\eta}{dy} + \eta \left(\frac{kf}{\omega h}\frac{dh}{dy} - \frac{f^2 - \omega^2}{gh} - k^2\right) = 0,$$
 (1)

where the x and y coordinates are in the alongshore (downstream) and the offshore directions, respectively (Fig. 2), η is the free surface elevation, k is the wavenumber along the x coordinate, ω is the frequency, g is the gravitational acceleration, h is the water depth, and f is the Coriolis frequency. The boundary conditions satisfy no normal flow at the coastal boundary and exponential decay of the SSH in the offshore direction outside the area of the variable depth (Huthnance, 1975; Zhang and Yankovsky, 2016).

We are using the MATLAB computational code developed by Yankovsky (2009) to solve the boundary problem. We have verified the results of this code against the results of the Fortran code developed by Brink and Chapman (1987), which is more cumbersome to use. The theory is used to compute dispersion relations as a function of cross-shore bathymetry profiles to determine the type of waves that propagate along narrow and wide shelves. For the HKE wave, the dispersion relation reflects a Kelvin wave at lower frequencies, an Edge wave at higher frequencies, and is almost a flat line at intermediate frequencies (Ke and Yankovsky, 2010), i.e., alongshore group velocity is nearly zero. For a given cross-shore transect, we use Eq. (1) to compute the eigenvectors of SSH for zero mode barotropic waves at the M₂ frequency. The zero mode has a SSH amplitude without a zero crossing along the cross-shore transect. The eigenvector of SSH is used to calculate the eigenvector of alongshore velocity as in Ke and Yankovsky

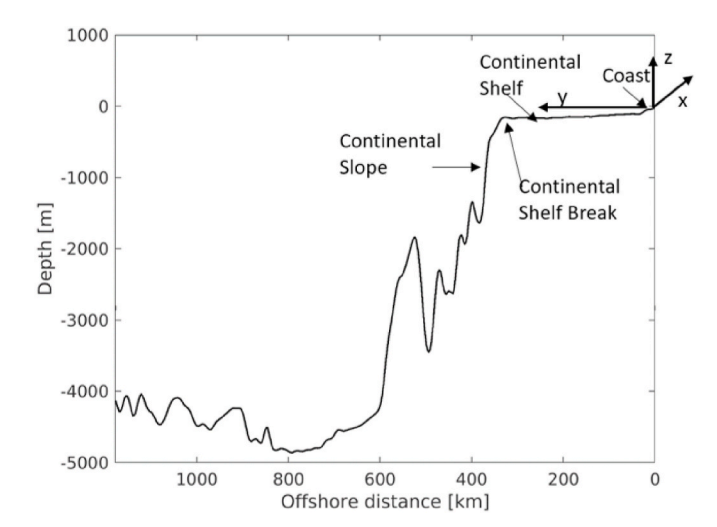


Fig. 2. The bathymetry along a zonal transect across the Celtic Sea/Bay of Biscay shelf at 48.5° N extracted from the global Hybrid Coordinate Ocean Model (HYCOM) simulation.

(2010). These eigenvectors will be fitted to the M_2 harmonic constants of SSH and alongshore velocity, obtained from the global and regional simulations discussed in the following sections.

2.2. Global baroclinic HYCOM simulation

A global baroclinic Hybrid Coordinate Ocean Model (HYCOM) simulation is utilized to identify areas where a transition from Kelvin waves to HKE waves coincides with the generation of internal waves, i. e., an onshelf barotropic flux causes an offshelf baroclinic energy flux on the wide shelf. We are using bathymetry and a one-month time series of barotropic and baroclinic fields from the global HYCOM simulation, which has a horizontal resolution of 1/12.5° and 41 hybrid vertical layers. This model simulation is discussed in detail in Ansong et al. (2015) and Buijsman et al. (2020). The HYCOM simulation is run in forward (non-data-assimilative) mode. This simulation features realistic atmospheric and tidal forcing. The simulation employs a wave drag to account for the barotropic tide energy conversion to unresolved modes and to dissipate resolved internal tides. The wave drag is tuned to get the most accurate barotropic tides compared to observations (Jayne and St. Laurent, 2001; Ansong et al., 2015; Buijsman et al., 2020). The simulation also uses a Self Attraction and Loading (SAL) (Hendershott, 1972) term based on the SAL calculated from TPXO8-atlas. The SAL term captures effects due to deformation of the solid earth by the load of the ocean tide, and alteration of the gravitational potential due to the self-gravitation of both the ocean tide and the load deformed solid earth (Hendershott, 1972).

2.3. Regional barotropic HYCOM simulations

We perform quasi-realistic regional 1/25° barotropic HYCOM simulations to understand the impact of 2D complex bathymetry in the CB area on the HKE wave transition. In these simulations, we gradually change the realistic bathymetry of the CB to a more idealized bathymetry. We discuss the bathymetry for these simulations in the Results section (3.2.1). Our objective is to change the bathymetry so that we eventually obtain a pure HKE wave transition. We use the existing model setup by Jeon et al. (2019), which domain covers the northwestern

Atlantic (Fig. 3). This model is one-way forced with SSH and barotropic velocity from a global HYCOM model simulation. The global simulation is forced with eight tidal constituents (M₂, S₂, K₁, O₁, N₂, P₁, K₂, and Q₁), but it does not have a realistic atmospheric forcing. The regional simulations are run for 29 days. We utilize the last 15 days for our analysis. The SAL term and wave drag used in Jeon et al. (2019) are set to zero in our simulations because these fields are cumbersome to recompute for the modified bathymetry. We found that the omission of these fields slightly affects the SSH and velocity amplitudes but has no effect on the energy flux patterns (results not shown). The root mean square (RMS) difference with and without SAL for the SSH amplitude is 1.44% for the shallow ocean (depth less than 250 m) and 1.36% for the entire domain. The RMS difference with and without wave drag for the SSH amplitude is 3.62% for the shallow ocean and 3.31% for the entire domain. However, we are recomputing quadratic bottom drag for all simulations with an altered bathymetry because damping the tides in shallow water is important. For all experiments, the bottom friction C_d is computed for seafloor depths shallower than 60 m according to (Schlichting, 1968; Buijsman et al., 2015)

$$C_d = \left\lceil \frac{\kappa}{\log\left(\frac{0.5h}{z_0}\right)} \right\rceil^2,\tag{2}$$

$$\kappa = 0.4, z_0 = 10 \text{ mm},$$
 (3)

where κ is the von Karman coefficient and z_0 is the bottom roughness. For the deep ocean (h>60 m), the quadratic drag coefficient is set to 0.0025.

2.4. Methodology

We compute the $\rm M_2$ harmonic constants for the SSH and horizontal barotropic velocities from the global and regional HYCOM simulation time series with a harmonic least-squares fit. The SSH and alongshore velocity from the global and regional HYCOM simulations are used to fit the theoretical eigenvectors of the zero mode SSH and alongshore velocity and calculate barotropic energy fluxes. The barotropic energy

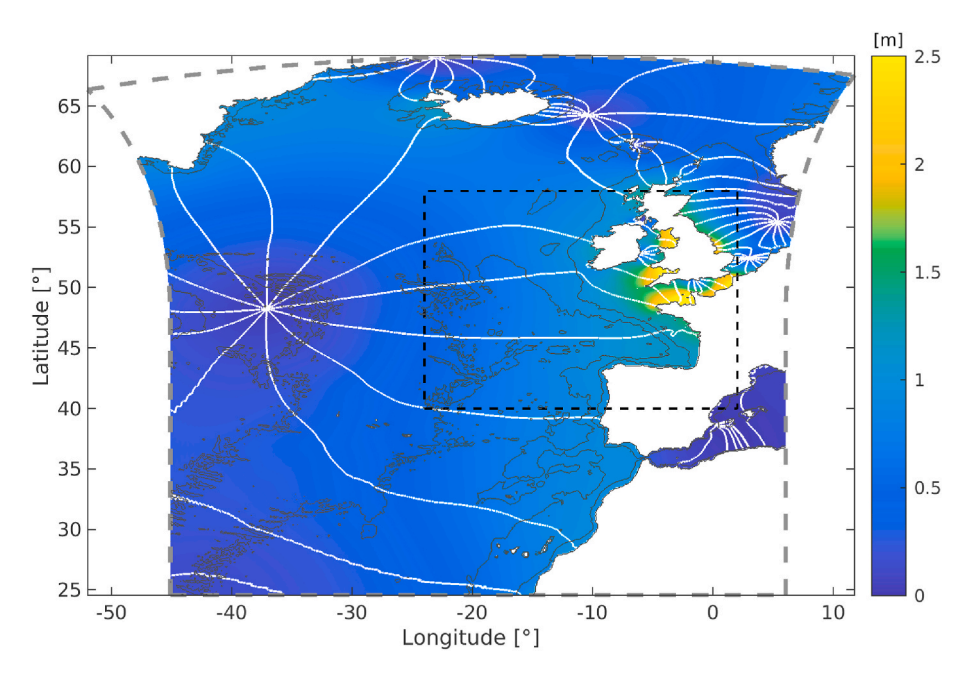


Fig. 3. M_2 Cotidal map (amplitude and phase) of SSH for the domain used for the regional barotropic HYCOM simulations. The outer gray dashed polygon marks the extent of the domain. The black dashed box shows the area where bathymetry is modified for our experiments. The bathymetry contours are plotted at 250 m and 4000 m depth as gray lines. The phases are the white lines plotted every 30° .

fluxes help us identify if the flux pattern associated with the HKE wave transition is present in the simulations. The time-mean barotropic energy flux is calculated as

$$(\overline{F_x}, \overline{F_y}) = \frac{1}{T} \int g\rho \eta(u, v) h dt$$

$$= \frac{1}{2} g\rho h \widetilde{\eta}(\widetilde{u} \cos(\varphi_{\eta} - \varphi_u), \widetilde{v} \cos(\varphi_{\eta} - \varphi_v)),$$
(4)

where u and v are the barotropic velocities in the x and y directions, respectively, and $\rho=1025~{\rm kg~m^{-3}}$ is the seawater density, T is the tidal period, $\widetilde{\eta}$, \widetilde{u} , and \widetilde{v} are the harmonic amplitudes, and φ_{η} , φ_{u} , and φ_{v} are the phase lags of the SSH and barotropic velocities.

From the global baroclinic simulation, we also compute the depthintegrated and time-averaged M_2 baroclinic energy fluxes to determine if these fluxes originate from wide shelves where the HKE wave transition may play a role. The time-mean and depth-integrated energy fluxes are calculated as (Nash et al., 2005; Buijsman et al., 2020)

$$\begin{split} (\overline{F_{x}'}, \overline{F_{y}'}) &= \frac{1}{T} \iint (u^{'}, v^{'}) p^{'} dz dt \\ &= \frac{1}{2} \int \widetilde{p}^{'} (\widetilde{u}^{'} \cos(\varphi_{u}^{'} - \varphi_{p}^{'}), \widetilde{v}^{'} \cos(\varphi_{v}^{'} - \varphi_{p}^{'})) dz, \end{split} \tag{5}$$

where z is the vertical coordinate, u' and v' are the horizontal baroclinic velocities in the x and y directions, respectively, p' is the perturbation pressure, \widetilde{u}' , \widetilde{v}' and \widetilde{p}' are the harmonic amplitudes, and φ_u' , φ_v' and φ_p' are the phase lags of the baroclinic velocities and perturbation pressure, respectively.

From the theory, we compute dispersion relations and M_2 SSH and alongshore velocity eigenvectors for the zero mode waves at selected cross-shelf bathymetry transects. For each shelf area, we pick one transect where the shelf is narrow and one where the shelf is wide. The transects are chosen perpendicular to the tidal wave propagation directions. In this way, the phase will be approximately constant along the transect. The realistic bathymetry for these transects is obtained from the HYCOM simulations. The minimum water depth for the bathymetry profile is 5 m. The realistic bathymetry is not a smooth curve, and some topographical features exist that may introduce noise in the results (Fig. 2). Hence, the bathymetry profile is smoothed by manually removing large bumps and then interpolating the depth in these areas to improve the accuracy. The seafloor is made flat seaward of the continental rise to exclude mid-ocean ridges.

We calculate the dispersion relation for these transects to identify whether the wave at the M_2 frequency is a Kelvin or HKE wave. The SSH eigenvector of the zero mode wave is extracted at the point where the dispersion curve intersects the M_2 frequency. The alongshore velocity eigenvector is calculated using the linearized momentum equations and the SSH eigenvector as in Ke and Yankovsky (2010).

The eigenvectors of SSH and alongshore barotropic velocity are linear least-squares fitted to the complex harmonic constants of the HYCOM $\rm M_2$ SSH and alongshore barotropic velocity to extract the $\rm M_2$ zero mode harmonic constants. The absolute values of the fitted harmonic constants are compared to those from the HYCOM simulations. Moreover, the mean ratio of the variance of the fit to the total variance (coefficient of determination) for each transect for the free surface elevation and alongshore velocity is calculated as

$$R^{2} = \frac{1}{n} \sum_{i=1}^{n} \left(1 - \frac{\sum_{j=1}^{m} (\gamma_{ij} - \widehat{\gamma}_{ij})^{2}}{\sum_{j=1}^{m} \gamma_{ij}^{2}} \right), \tag{6}$$

where $\hat{\gamma}$ and γ are the time series of the fit and HYCOM simulation, respectively, n is the number of points i along the transect, and m is the number of time steps j.

We use the zero mode fitted harmonic constants of SSH and barotropic velocities to compute the alongshore time-mean barotropic energy flux to compare with the M_2 flux in the HYCOM simulation. The alongshore zero mode energy flux is calculated according to two methods. In method I, the actual SSH and alongshore velocity phase lags are considered, whereas in method II, the phase difference between SSH and alongshore velocity is considered zero if their eigenvectors have the same sign; otherwise, they are considered out of phase. In method I, the wave may be partially progressive, while we assume the wave is purely progressive in method II.

3. Results

3.1. Identification of shelf areas with HKE wave transition

One of our goals is to identify shelf areas in the global baroclinic HYCOM simulation where the transition from M_2 barotropic Kelvin waves into HKE waves coincides with onshelf barotropic and offshelf baroclinic energy fluxes. Hence, we analyze the coastal areas where the shelf widens and large cross-shore barotropic and baroclinic energy fluxes are present. The time-mean and depth-integrated barotropic energy fluxes are shown for the global ocean in Fig. 4. We have highlighted coastal areas with a red curve where phase lines in Fig. 4 reflect progressive Kelvin waves. We exclude coastal areas with offshore standing tidal waves (e.g., Northwest Australia, Gulf of Alaska), or where the phase propagation is opposite to Kelvin wave propagation (e.g., Southwest Africa), and areas with many islands and inlets (e.g., Southeast Asia).

We compute the shelf width, cross-shore barotropic, and baroclinic fluxes to identify widening shelf areas where the HKE wave transition may generate strong internal tide beams. The shelf width is calculated by assuming the shelf break occurs at the 500 m isobath. This depth is chosen for the shelf break because a smoother contour is obtained at 500 m depth. Since the depth increases very rapidly seaward of the shelf break, this choice does not lead to any considerable errors in the shelf width. The cross-shore barotropic and baroclinic fluxes are calculated at the 1500 m isobath because we want to capture the offshelf propagating internal tides, which are primarily generated in shallower water depths, i.e., on the slope between 1000 m and the shelf break. Barotropic and baroclinic fluxes perpendicular to the 1500 m isobath are considered cross-shore.

The cross-shore barotropic and baroclinic fluxes are plotted against shelf width in Fig. 5 for the coastlines highlighted in red color in Fig. 4. If the direction of the flux is onshelf (offshelf), then it is considered positive (negative). The onshelf barotropic fluxes > 100 kW m⁻¹ and offshelf baroclinic fluxes $> 1 \text{ kW m}^{-1}$ coincide with shelf widths > 150 km. In western Europe, we observe a strong onshelf barotropic and offshelf baroclinic flux at the CB shelf. Here, the shelf also becomes very wide (around 380 km). The distance to the opposite coast (North America) is greater than the Rossby radius of deformation ($R_f = c/f = 1850$ km, where *c* is the phase speed for a long gravity wave). The amplitude of the Kelvin wave becomes negligible when the distance from the coast becomes equal to the Rossby radius of deformation. This means that the opposite coast is not affected by the Kelvin wave in this region. An onshelf barotropic and offshelf baroclinic flux is also observed at the Queen Charlotte shelf on the west coast of North America. The Amazon shelf also shows a strong onshelf barotropic and offshelf baroclinic energy flux. A weak onshelf barotropic and offshelf baroclinic energy flux exist at the wide Sierra Leone shelf on the west coast of Africa. However, $R_f = 11650$ km is larger than the width of the Atlantic basin at this latitude. Hence, the Kelvin wave on the opposite coast affects the SSH on both Amazon and Sierra Leone shelves. A HKE wave occurs on the very wide and narrowing Patagonia shelf (Ke and Yankovsky, 2010), but since this wave does not scatter much baroclinic energy offshelf (Buijsman et al., 2020), it is omitted from our analysis. For the Gulf of Alaska shelf, a propagating Kelvin wave exists on the narrow shelf. However, the tidal wave may be partially progressive for the wide shelf, causing the phase lines to be oblique to the shore rather than

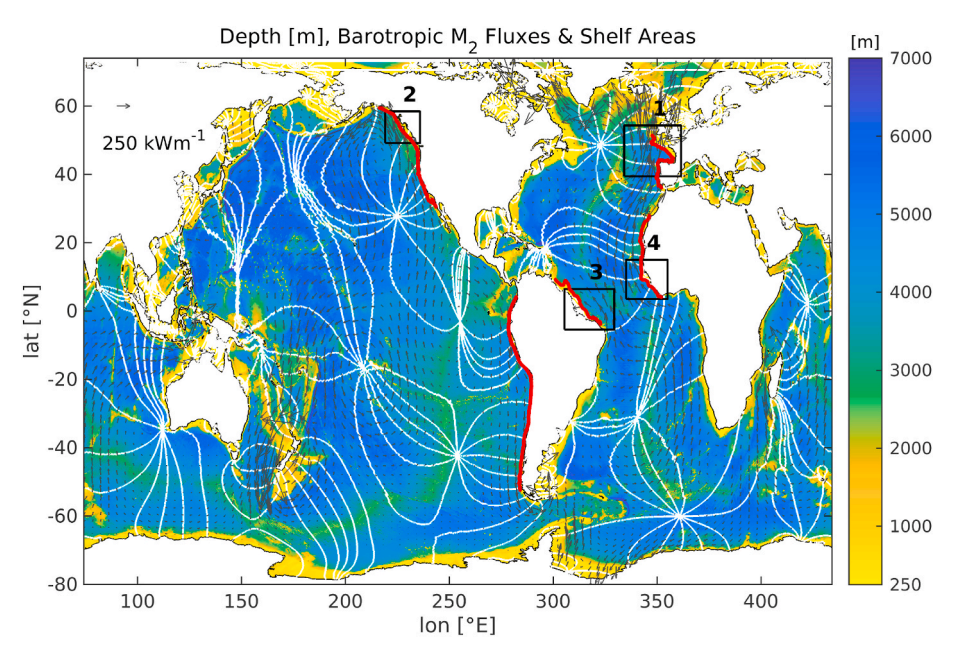


Fig. 4. Global map with M₂ barotropic energy fluxes (vectors), seafloor depth (colors), M₂ phase plotted every 30° (white contours), and shelf areas where the Kelvin - HKE wave transition may occur (numbered boxes: 1. Celtic Sea/Bay of Biscay shelf, 2. Queen Charlotte shelf, 3. Amazon shelf, and 4. Sierra Leone shelf).

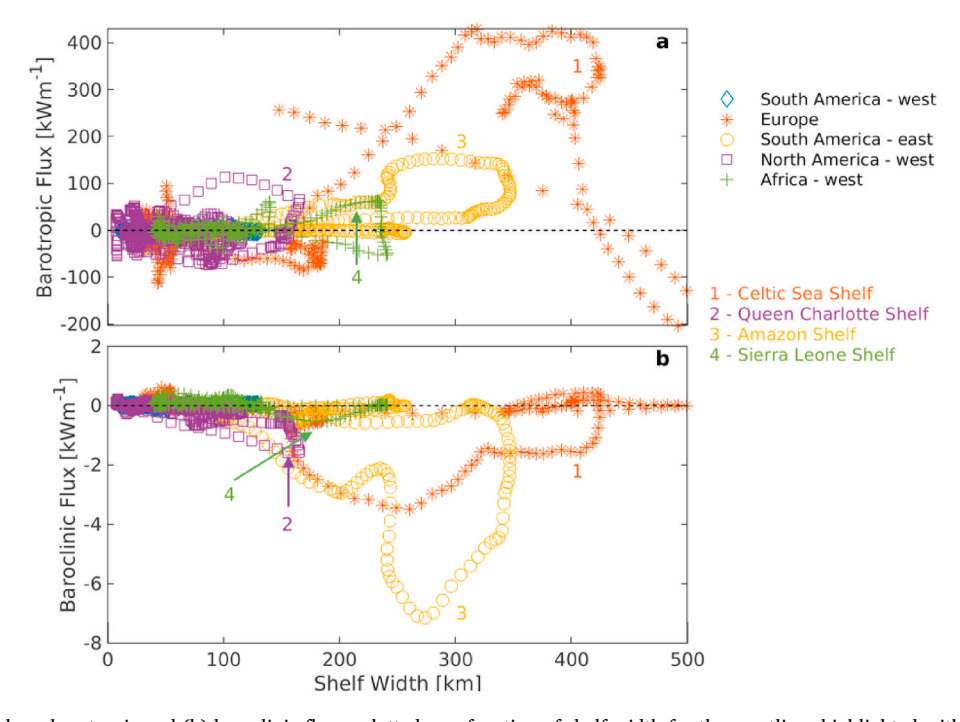


Fig. 5. (a) The cross-shore barotropic and (b) baroclinic fluxes plotted as a function of shelf width for the coastlines highlighted with the red line in Fig. 4.

perpendicular. The barotropic energy fluxes are parallel to the phase lines in the deep ocean offshore of this shelf area, confirming the presence of a standing wave. In the following, we analyze two shelves in more detail - the CB and Queen Charlotte shelves. These shelves widen in the alongshore propagation direction, and they feature relatively large onshelf barotropic and offshelf baroclinic energy fluxes (Fig. 5).

3.1.1. Celtic Sea/Bay of Biscay and Queen Charlotte shelves

To better understand the relation between the barotropic and baroclinic tides, we show the cotidal maps and the depth-integrated barotropic and baroclinic energy fluxes for the CB and Queen Charlotte shelves in Fig. 6. As observed from Fig. 6b, the direction of the

barotropic energy flux is along the narrow shelf of the west coast of the Iberian peninsula, and it changes towards the shore as the shelf widens in the Celtic Sea. Fig. 6c shows the radiation of semidiurnal baroclinic energy flux in the offshelf direction where the continental shelf widens in the CB. The Queen Charlotte shelf widens in the alongshore propagation direction; however, the onshelf barotropic (Fig. 6e) and offshelf baroclinic fluxes (Fig. 6f) are weaker compared to the fluxes of the CB shelf.

3.1.2. Dispersion relation

We evaluate the wave dispersion relations along the transects in Fig. 6b and e to identify the type of wave present on the narrow and wide

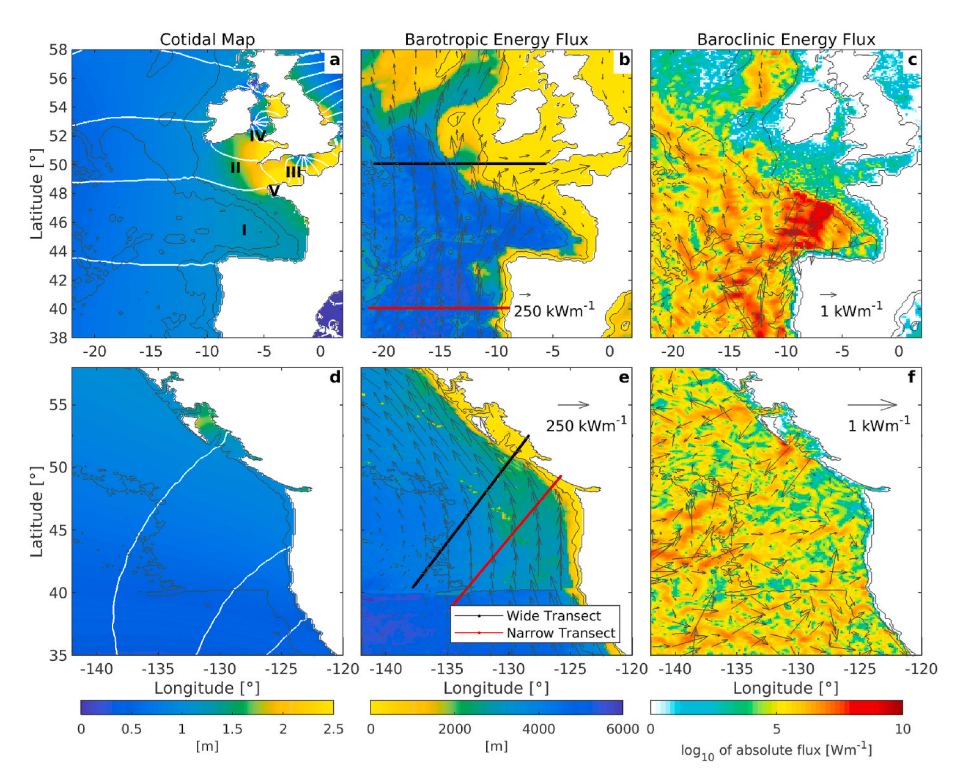


Fig. 6. M_2 cotidal map (SSH amplitude and phase; left), barotropic energy fluxes (middle), and baroclinic energy fluxes (right) for the selected shelf areas: (a–c) the Celtic Sea/Bay of Biscay Shelf and (d–f) the Queen Charlotte Shelf. In the cotidal maps, phases are plotted every 30° as white contours. In (b) and (e), the location of two transects is shown across a narrow and wide shelf. In (c) and (f), the colormap shows the \log_{10} of baroclinic energy flux. In (a), I marks the Bay of Biscay canyon, II marks the Celtic Sea shelf, III marks the English Channel, IV marks the St. George's Channel, and V marks Brittany. Black contours are plotted at 250 m and 4000 m depth.

CB and Queen Charlotte shelves (Fig. 7). At the narrow shelves, we observe a Kelvin wave at the M2 frequency for both regions, where red lines intersect the M2 frequency. At the wide shelf of the CB, we see a transition from a Kelvin wave to a HKE wave, which is characterized by the flattening of the slope of the dispersion curve at the M2 frequency (Fig. 7a). At this point, the group velocity approaches zero, indicating an arrest of the alongshore wave propagation and potential offshore radiation of wave energy. However, this transition does not happen for the Queen Charlotte shelf, where the dispersion diagram still shows a Kelvin wave at the M₂ frequency for the wide shelf (Fig. 7b). We also compute the dispersion relation at the wide Sierra Leone shelf (not shown). We find that at the M2 frequency, the shelf is wide enough to feature a HKE wave. However, a Kelvin wave traveling along the opposite coast produces a signal on this shelf because the ocean basin width is smaller than R_f . We do not compute the dispersion relation for the Amazon shelf. This shelf is at the equator and the Coriolis frequency changes its direction

along the transect, and it is difficult to evaluate the wave dispersion relation. We do not analyze the Sierra Leone and Amazon shelves any further, and we focus on the CB shelf only.

3.1.3. Fitting the zero mode eigenvectors

In the following, we fit the zero mode SSH and velocity eigenvectors from the theory to the SSH and alongshore barotropic velocity harmonic constants from the global baroclinic HYCOM simulation for the CB shelf. The fitting is done to determine how much of the tidal variance in the HYCOM simulation is due to these zero modes.

The fitted zero mode SSH and barotropic energy flux for the transect on the narrow shelf for the CB shows a good agreement with the HYCOM simulation in Fig. 8 (left column). However, the on-shelf comparison of alongshore velocity does not show a good agreement (Fig. 8e). The root mean square (RMS) of the tidal-mean barotropic energy flux along the transect for HYCOM simulation is $472~\mathrm{kW}~\mathrm{m}^{-1}$, and agrees well with the

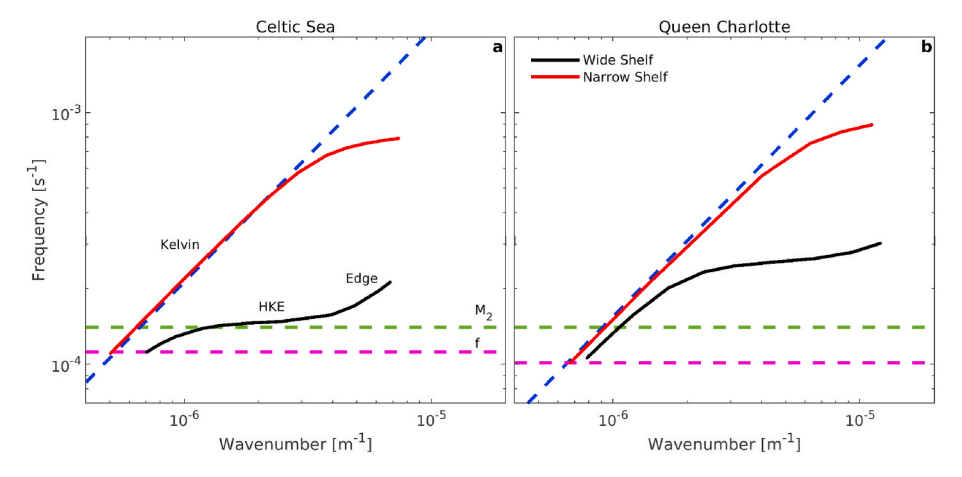


Fig. 7. The dispersion relations at the narrow and the wide shelf of (a) the Celtic Sea/Bay of Biscay and (b) Queen Charlotte. The green and magenta lines indicate the M₂ and inertial frequencies, respectively. The blue dotted line is the dispersion relation of a surface Kelvin wave for a constant seafloor depth of (a) 4500 m and (b) 2400 m.

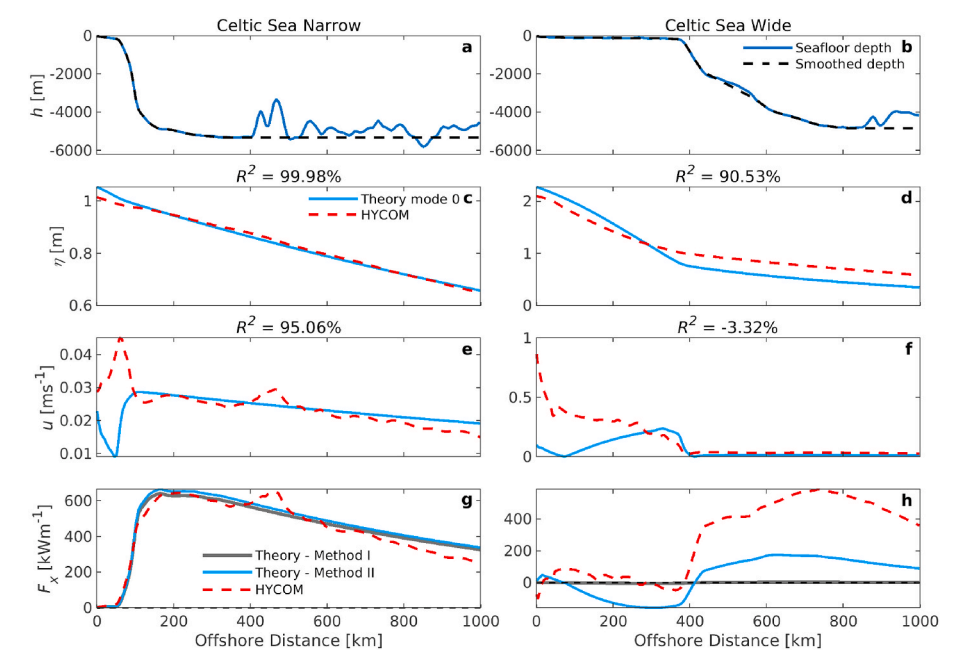


Fig. 8. (a)–(b) The seafloor depth along the transect, (c)–(d) SSH amplitude, (e)–(f) alongshore barotropic velocity amplitude, and (g)–(h) alongshore barotropic flux for the narrow shelf (left column) and the wide shelf (right column) of the Celtic Sea/Bay of Biscay area. In (a)–(b), the black dashed line marks the bathymetry used for the eigenmode calculation. In (c)–(f), the fitted zero mode amplitudes are the blue and the HYCOM amplitudes are the red lines. In (g)–(h), the gray (blue) line represents the zero mode flux computed according to method I (method II), and the red line shows F_x from the HYCOM simulation. R^2 represents the fraction of the variance of the HYCOM simulation captured by the fit (Eq. (6)).

RMS of the fitted tidal-mean barotropic energy flux of 478 kW m⁻¹ and 496 kW m⁻¹ for methods I and II, respectively (see section 2.4). The good agreement between these RMS values and the flux curve implies a progressive Kelvin wave is present on the narrow shelf (Fig. 8g). The trends of the SSH and alongshore velocity for the fitted zero mode are similar to the HYCOM simulation on the wide shelf (Fig. 8, right column). However, the values for the fitted barotropic energy fluxes are much smaller as compared to the HYCOM fluxes (Fig. 8h). The along transect RMS of the tidal-mean barotropic energy flux for the HYCOM simulation is 369 kW m⁻¹, whereas the RMS of the fitted zero mode energy fluxes for methods I and II are 3 kW m⁻¹ and 127 kW m⁻¹, respectively. The flux trends in Fig. 8h and the RMS value for method II are in better agreement with the HYCOM simulation, which implies that the fit of method I has characteristics of a standing wave. We observe characteristics of a HKE wave in the HYCOM simulation, as predicted by the theory, but the differences may be attributed to two-dimensional (2D) bathymetry or bottom friction not accounted for with the linear theory for a 1D transect.

3.2. Sensitivity of HKE wave mechanism to complex bathymetry

To better understand the effects of 2D bathymetry on the HKE wave transition, we perform quasi-realistic regional $1/25^{\circ}$ barotropic HYCOM simulations of the CB. Of all the wide shelf areas considered, the CB has the widest shelf and the largest cross-shore barotropic and baroclinic energy fluxes. This shelf potentially features a HKE wave transition and associated internal wave generation.

3.2.1. Description of experiments

We change the bathymetry of the CB from realistic to idealized in a series of steps for the regional HYCOM simulations. This is done to understand how the incident Kelvin wave is affected by various topographic features, such as the widening shelf, the English and St George's Channels, and the Bay of Biscay canyon (for the names of all geographic features, see Fig. 6a). These experiments are explained in Table 1, and the experiment bathymetries, except experiment 2, are shown in Fig. 9. The original bathymetry is used for experiment 1. The deep ocean is made flat with a seafloor depth of 4000 m for the remaining experiments. The English and St George's Channels are closed for experiments 3 to 7. In experiments 5, 6, and 7, the shelfbreak contour is rotated

Table 1The details of regional model simulation experiments performed in the Celtic Sea/Bay of Biscay Area.

Exp No.	Changes in Bathymetry
1	Original bathymetry is used
2	Deep ocean is made flat with a depth of 4000 m
3	As experiment 2, but the English and St. George's Channels are closed
4	As experiment 3, but the shelf and the Bay of Biscay coast are extended seaward to remove the canyon
5	As experiment 4, but the shelf break is straightened
6	As experiment 5, but the land is extended seaward at the wide shelf, and the coast is made parallel to the shelf break. The width of the wide shelf is 225 km.
7	As experiment 6, but Ireland is removed to increase the alongshore length of the wide shelf, and the width of the wide shelf is increased. The width of the wide shelf is 375 km.

clockwise to ensure the deep-water barotropic waves propagate along and not across the shelf break.

3.2.2. Barotropic energy flux patterns

We evaluate the barotropic energy flux patterns for the experiments shown in Table 1 to better understand the effect of the 2D bathymetry on the HKE wave. The barotropic energy flux patterns are shown in Fig. 9 for all the experiment bathymetries. We also average the onshelf and offshelf barotropic energy flux along the 250 m isobath at the wide shelf (Table 2). This is done to determine whether the strong cross isobath fluxes are due to the HKE wave conversion or topographic features such as the canyon, and the English and St. George's Channels. We are also evaluating alongshore and cross-shore fluxes and cotidal maps for experiments 3, 4, and 7 in detail in Fig. 10.

The flux patterns are similar for experiments 1 and 2 (Fig. 9a and Table 2). We conclude that the flat ocean bottom is not impacting the flux patterns. In both experiments, an onshelf flux is directed towards the English and St. George's Channels. A south-eastward flux is present on the shelf south of Brittany in experiment 1 (Fig. 9a). The clockwise flux pattern featuring the onshelf and southward fluxes somewhat resembles the HKE wave flux pattern in Fig. 1 and in the idealized model simulations in Fig. 6 of Yankovsky and Zhang (2017), but the southward flux in experiment 1 is much weaker than the onshelf flux, i.e., the flux in

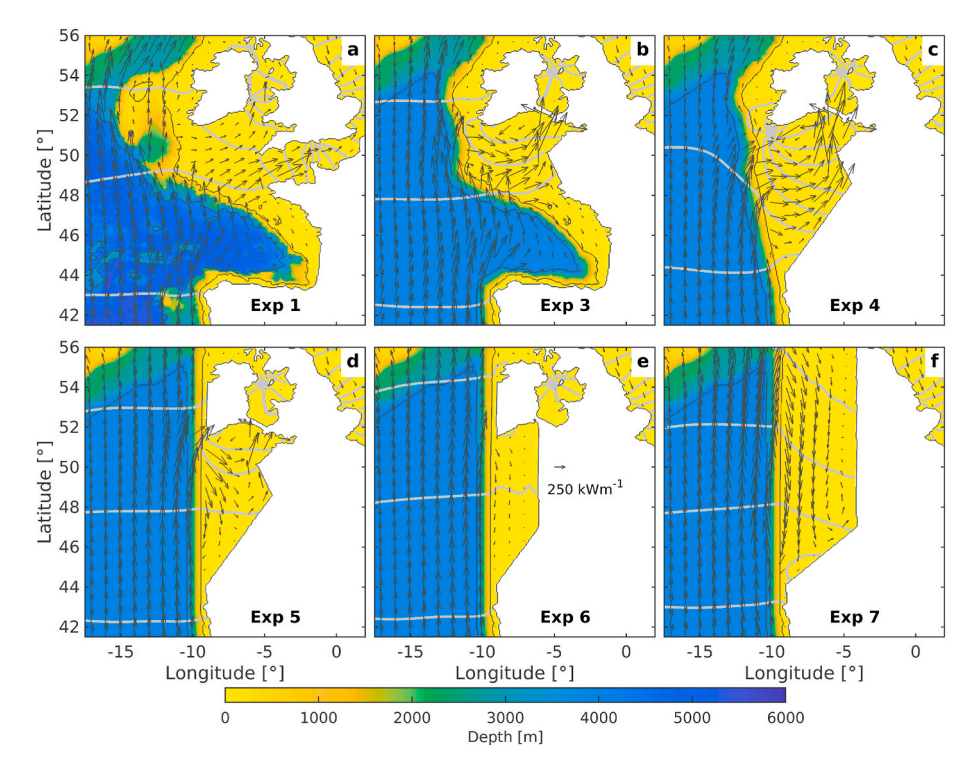


Fig. 9. The bathymetry configurations for the experiments in the Celtic Sea/Bay of Biscay area with the M₂ barotropic energy flux vectors and SSH phases (gray contours plotted every 30°). Black bathymetry contours are plotted at 250 m and 4000 m.

Table 2The comparison of cross-shore fluxes on the wide shelf for experiments 1–7.

Exp. no.	Onshelf Flux per unit length (kW m ⁻¹)	Offshelf Flux per unit length (kW m ⁻¹)	Length along shelf break over which fluxes are calculated (km)	Range of latitude along shelf break over which fluxes are calculated (° N)
1	111	-10	1230	44.82–51.19
2	116	-10	1176	44.82-51.19
3	166	-17	1176	44.82-51.19
4	271	-2	824	44.09-51.19
5	134	-29	781	44.09-51.19
6	13	-20	781	44.09-51.19
7	126	-27	1560	44.09–58

the HKE wave circulation pattern is not conserved.

In experiment 3, we close the English and St. George's Channels, and in experiment 4, we also remove the canyon (Fig. 9b and c). Compared to experiment 1, the onshelf flux on the wide shelf and the SSH amplitude have increased in experiments 3 and 4 (Fig. 9b and c, Fig. 10a and e). In experiment 4, the average onshelf flux along the shelf break is 271 kW m⁻¹, and it is the largest of all the experiments (Table 2). In both experiments 3 and 4, we attribute the increase in flux and amplitude to a standing tidal wave modified by rotation, which is characterized by a large SSH amplitude at the coastal boundary (Fig. 10a and e) and onshelf fluxes that are parallel to the phase lines on the wide shelf (Fig. 9b and c). The additional effect of extending the wide shelf area in experiment 4 is that the standing wave pattern has expanded southwards. In experiment 4, the width of the shelf $W \approx 340$ km and the average depth of the shelf h = 90 m. The natural period for this semi-enclosed shelf $T_e = 4W/$ \sqrt{gh} = 12.71 h (Knauss and Garfield, 2016), which is close to the semidiurnal tidal period. This suggests that the shelf could be in resonance with the tidal forcing.

We straighten the shelf break in experiments 5, 6, and 7 (Fig. 9d, e, and f). In addition, Ireland is removed in experiment 7. Compared to experiment 4, the average onshelf flux of $134~\mathrm{kW~m}^{-1}$ along the shelf break is smaller in experiment 5 (Table 2). The main difference between

experiments 4 and 5 is that the shelf break makes a slightly oblique angle to the incident Kelvin wave in experiment 4 and that the shelf break is rotated clockwise in experiment 5. As a consequence, the shelf width is reduced in experiment 5. This change in shelf width results in different flux patterns in experiments 4 and 5. In experiment 5, the barotropic energy fluxes on the shelf are not parallel to the phase lines, and hence the standing wave phenomenon is not observed in this experiment (Fig. 9d). The clockwise flux patterns begin to resemble a HKE wave in this experiment, i.e., the flux is onshelf close to Ireland and offshelf at the southern boundary of the wide shelf. The average onshelf flux is small in experiment 6 (13 kW m⁻¹) because the shelf is not sufficiently wide to facilitate a strong HKE wave (Fig. 9e and Table 2). In experiment 7, Ireland is removed to increase the alongshore length of the wide shelf, and the width of the wide shelf is increased (Fig. 9f). After the removal of Ireland, the flux recirculation pattern is strengthened and extended towards the north. In this experiment, there is a strong upstream (southward) barotropic energy flux on the wide shelf. Moreover, in experiment 7, there is no alongshore variation in the shelf width. Hence, the flux pattern in Figures 9f and 10k and l is very similar to the pattern in Fig. 1 and the idealized model simulations in Fig. 6 of Yankovsky and Zhang (2017). The upstream flux on the wide shelf is blocked by the coast where the shelf widens, just north of the Iberian Peninsula, and it is directed offshelf. Similar to Yankovsky and Zhang (2017), a downstream (northward) alongshore flux is also present adjacent to the coast (Fig. 10k).

We also modify the bathymetry of experiment 7 by including the canyon and the English Channel to understand their impact on the HKE wave transition (Appendix A). The addition of the canyon reduces the alongshore length of the wide shelf. Moreover, the inclusion of the English Channel increases the onshore flux. However, for this idealized experiment, neither the canyon nor the English Channel significantly impacts the HKE wave flux pattern.

From these idealized experiments, we conclude that the barotropic energy flux patterns of the HKE wave are sensitive to topographic features and may be masked by fluxes due to other processes. The flux patterns in experiment 1 somewhat resemble a HKE wave, with a strong

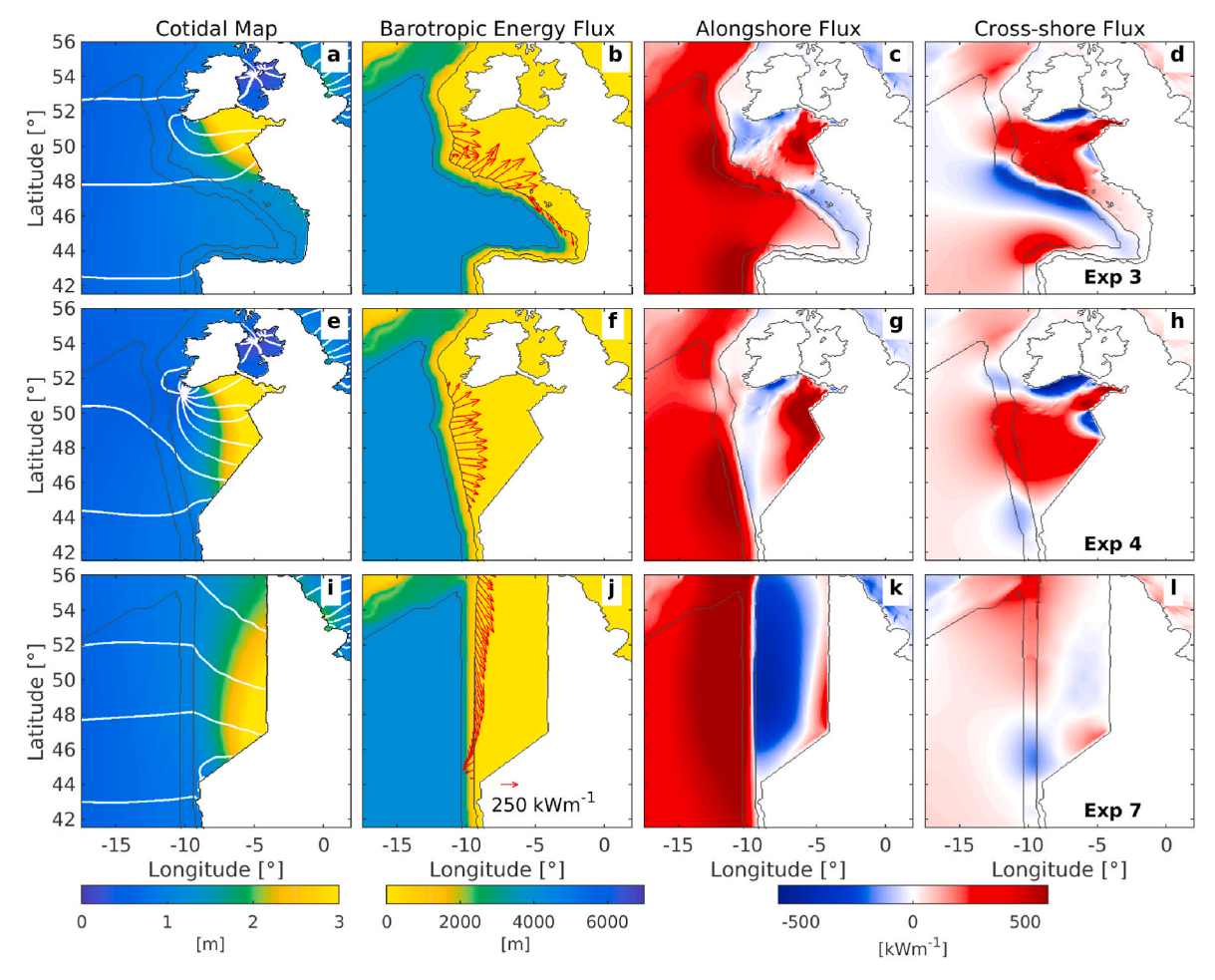


Fig. 10. Model results for (a–d) experiments 3, (e–h) 4, and (i–l) 7. The first column shows the M_2 amplitude and phase plotted every 30° (white contours), the second column shows the Celtic Sea/Bay of Biscay bathymetry with the M_2 barotropic energy flux vectors at the shelf break, the third column shows the alongshore barotropic energy flux (positive is to the north), and the fourth column shows the cross-shore barotropic energy flux (positive is to the east). Black bathymetry contours are plotted at 250 m and 4000 m.

onshelf flux on the downstream side of the circulation cell, but with only a small fraction of the onshelf flux directed upstream. The HKE wave flux pattern is thus greatly modified by 2D topographic effects due to the English and St George's Channels, the canyon, the orientation of the shelf break relative to the incident Kelvin wave, the shelf width, and standing wave features.

3.2.3. Dispersion relation

We calculate the dispersion relations for the most idealized experiments 6 and 7 for the narrow and wide shelf transects (Fig. 11) to verify if the theory predicts Kelvin and HKE waves for these experiments. The dispersion relations for experiments 6 and 7 show the presence of a Kelvin wave on the narrow shelf. While the shelf in experiment 6 is not

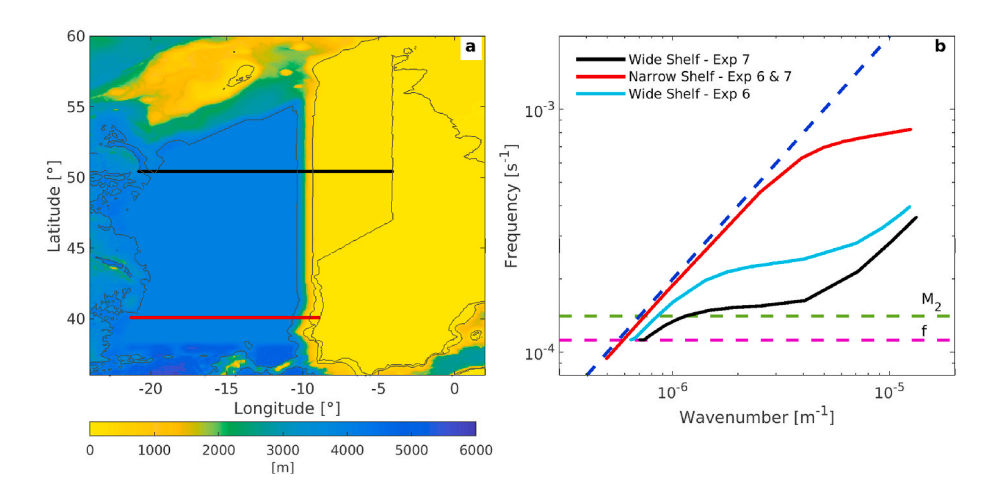


Fig. 11. (a) The location of two transects at the narrow and wide shelves for experiment 7. The transect locations are the same for experiment 6. (b) The dispersion relation for the narrow and wide shelves for experiments 6 and 7.

wide enough to facilitate a HKE wave ($W=225~{\rm km}$), a HKE wave is present in experiment 7 ($W=375~{\rm km}$) according to the dispersion relation in Fig. 11b. In experiment 7, the group velocity for the wide shelf is close to zero at the semidiurnal frequency, which is in agreement with the flux patterns shown in Fig. 9f. From dispersion calculations for different shelf widths, we find that a HKE wave exists at the M_2 frequency for shelf widths of at least 300 km.

3.2.4. Fitting the zero mode eigenvectors

As in section 3.1.3, we fit the zero mode eigenvectors of SSH and alongshore velocity to harmonic constants of SSH and alongshore velocity of experiment 7 to determine if a HKE wave transition exists in this experiment. For experiment 7, SSH, alongshore velocity, and barotropic energy flux for both the fitted zero mode and HYCOM simulations are in agreement for both narrow and wide shelves (Fig. 12). The coefficient of determination R^2 for the SSH and alongshore velocity for both transects is higher in experiment 7 than in experiment 1 (not shown) and the global HYCOM simulation (Fig. 8). This is expected because the wide shelf bathymetry for experiment 7 is 1D over an alongshore distance of 100s of km. The good agreement between experiment 7 and the theory proves that the effect of bottom friction on the HKE wave transition is small. We observe some differences for the alongshore velocity in shallow water on the wide shelf, but they are minor (Fig. 12f). For the original bathymetry, the agreement on the wide shelf between the HYCOM simulations and the theory is less (Fig. 8) because the HKE wave transition is sensitive to the complex 2D topography.

3.2.5. Phase speed comparison

It follows from the dispersion curve that the HKE wave has an alongshore group velocity that is close to zero $(c_g = \partial \omega/\partial k \approx 0)$ and that its phase speed $(c = \omega/k)$ is reduced due to a larger wavenumber as compared to the Kelvin wave. To identify Kelvin and HKE waves along the narrow and wide shelves of the CB, we compute the phase speed with a Hovmöller diagram of HYCOM M₂ SSH for alongshore transects on the shelf and off the shelf in deep water. The phase speed for the theory is calculated where the dispersion curve intersects the M₂ frequency. We compute phase speeds for experiments 1 and 7 (Table 3).

The phase speed is higher for the narrow shelf than the wide shelf for both the HYCOM experiments and the theory. Since the narrow shelf features a Kelvin wave, the phase speed can also be calculated with c=

Table 3 The comparison of phase speeds calculated from HYCOM M_2 SSH and the theory. The values in parenthesis represent the relative change in phase speed from the narrow to the wide shelf.

Phase Speed	НҮСОМ				Theory	
(m s ⁻¹)	Off Shelf		On Shelf		'	
	Narrow	Wide	Narrow	Wide	Narrow	Wide
Experiment 1 Experiment 7	240 198	155 (-35%) 127 (-36%)	306 251	90 (-71%) 129 (-49%)	219 189	116 (-47%) 123 (-35%)

 \sqrt{gh} , where h is the water depth for the deep ocean. For h=5000 m in experiment 1, we find a phase speed $c=\sqrt{gh}=221$ m s⁻¹, which is close to the theoretical phase speed of 219 m s⁻¹. For h=4000 m in experiment 7, the phase speed calculated from the theory is 189 m s⁻¹, which is close to $\sqrt{gh}=200$ m s⁻¹.

Both the theory and HYCOM experiments 1 and 7 show a significant reduction in the phase speed from the narrow to the wide shelf for both off-shelf and on-shelf transects (Table 3). We also find that the SSH-inferred phase speeds of the idealized experiment 7 are in better agreement with the theory than the phase speeds of the realistic experiment 1. We conclude that the reduced phase speed is another indication a HKE wave is present on the wide shelf in the theory as well as in the realistic and idealized HYCOM experiments.

4. Discussions and conclusions

In this study, we investigate continental shelves in the global ocean where the Hybrid Kelvin-Edge (HKE) wave transition causes the offshore radiation of internal tides as postulated by Yankovsky and Zhang (2017). For this purpose, we use theory and realistic global baroclinic and quasi-realistic regional barotropic model simulations to understand the transition process of semidiurnal HKE waves at widening shelves.

Using the global baroclinic Hybrid Coordinate Ocean Model (HYCOM) simulation, we identify areas where a widening shelf in the alongshore (i.e., downstream) direction coincides with onshelf barotropic and offshelf baroclinic energy fluxes. Of all the widening shelf

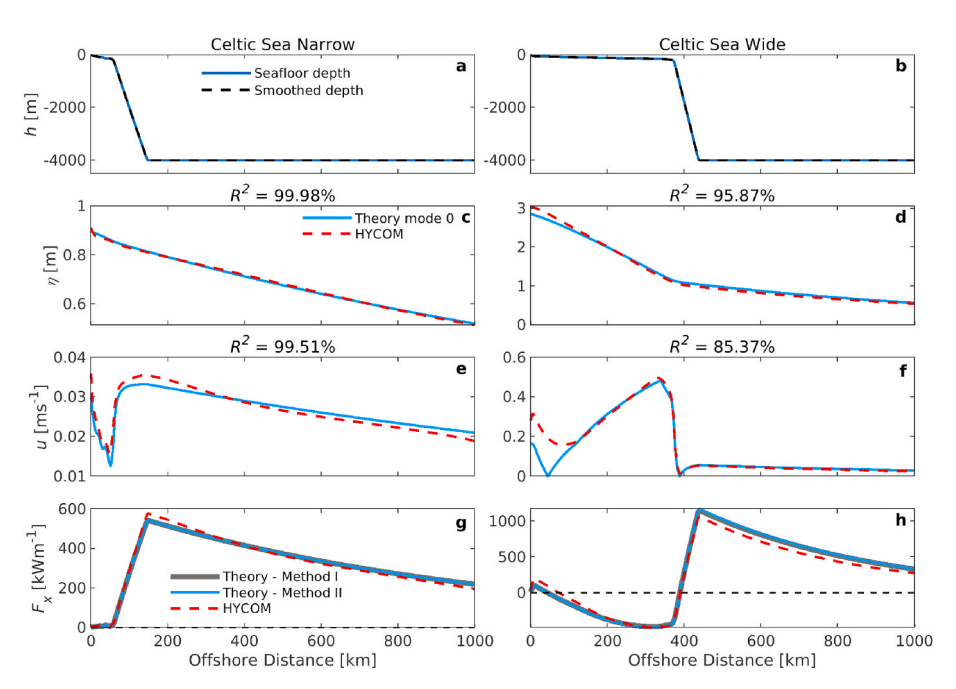


Fig. 12. The caption is same as in Fig. 8 but for experiment 7.

areas considered, the Celtic Sea/Bay of Biscay (CB) and Queen Charlotte shelves have the largest potential to feature a HKE wave that scatters internal tides offshore. Other shelf areas are affected by the Kelvin waves on the other side of the ocean basin (Sierra Leone and Amazon shelves) or do not radiate strong internal waves offshore (Patagonia shelf).

Next, we calculate dispersion relations for the CB and Queen Charlotte shelves to identify the type of HKE wave. For the CB shelf, it predicts the presence of a Kelvin wave on the narrow shelf (Portugal shelf region) and a HKE wave on the wide shelf. However, the Queen Charlotte shelf is not wide enough to support a HKE wave transition. For the CB shelf, we fit the zero mode SSH and alongshore velocity eigenfunctions to the $\rm M_2$ harmonic constants of the global HYCOM simulation to determine how much of the variance in the simulation is due to the zero mode. The fitted zero mode sea surface height (SSH) and velocity amplitudes, and energy flux agree well with the HYCOM simulation for the narrow shelf where a Kelvin wave is present. Although the width of the CB shelf is sufficient to support a HKE wave, the fitted modes do not agree well with the HYCOM simulation on the wide shelf.

To better understand the discrepancy, we perform a series of regional barotropic HYCOM simulations for the CB bathymetry configurations ranging from realistic to idealized. These simulations suggest that the complex 2D bathymetry of the CB modifies the HKE wave. In experiment 1, where a realistic bathymetry is used, we see some aspects of a clockwise barotropic energy flux pattern associated with a HKE wave transition, i.e., the downstream onshelf flux and the southward flux on the shelf south of Brittany (compare Figs. 1 and 9a). However, this flux pattern is significantly modified by the English and St. George's Channels, and topographic steering by the canyon and orientation of the shelf break. When the English and St. George's Channels are closed (experiment 3) and the canyon is removed (experiment 4), we observe enhanced SSH amplitudes and barotropic energy fluxes parallel to the phase lines. These are characteristics of a resonant standing wave. However, it is not clear from these experiments if a standing wave is present in experiments 1 and 2, and if it contributes to the onshelf flux. The standing wave patterns are not present in experiments 5 to 7, illustrating the standing wave is sensitive not only to the shelf width and friction (Clarke and Battisti, 1981; Arbic and Garrett, 2010) but also to 2D geometry. In Experiment 7, where the English and St. George's Channels are closed, the canyon is removed, and the shelf width is constant in the alongshore direction, we observe a clear HKE wave transition. In this experiment, which resembles the idealized configuration of Yankovsky and Zhang (2017), we compute the same clockwise barotropic energy flux pattern as shown in their Fig. 6.

We also calculate the dispersion relation and fit the zero mode eigenvectors to experiment 7 in the CB area at narrow and wide shelves. The dispersion relation predicts that a HKE wave is present on the wide shelf. The fitted zero mode SSH, alongshore barotropic velocity, and alongshore barotropic energy flux are also in good agreement with the experiment 7 simulation at both the narrow and wide shelves (i.e., R^2 approaches 100%).

As a Kelvin wave transitions to a HKE wave, the zero mode phase speed is reduced. Hence, we compare the downstream phase propagation as predicted by the theory with the phase speeds in deep water and on the shelf in the regional HYCOM experiments 1 (realistic) and 7 (idealized). In both the theory and the experiments, the phase speed decreases from the narrow to the wide shelf, indicating that a HKE wave is present on the wide shelf. For experiment 1, the agreement with the theory on the wide shelf is less, most likely because of the 2D topography complexity of the Celtic Sea.

The HKE wave transition features several barotropic energy flux circulation patterns that depend on the shelf widths of the narrow and wide shelves as discussed in Zhang and Yankovsky (2016) and Yankovsky and Zhang (2017). In this paper, we are mainly focusing on a clockwise flux pattern in which the alongshore energy flux changes its direction towards the shore on the downstream location of the wide shelf, and the energy flux is offshelf at the upstream location (Fig. 1). This flux pattern also features the generation of internal tides that radiate offshore. In the experiments by Yankovsky and Zhang (2017) that have this flux pattern, the width of the narrow and wide shelf is 150 km and 300 km, respectively, and the deep ocean depth is 2000 m. However, in our experiments, the width for the narrow shelf is 50 km, the width for the wide shelf varies from 225 km to 380 km, and the ocean is at least 4000 m deep. Zhang and Yankovsky (2016) and Yankovsky and Zhang (2017) did not perform an experiment in which the shelf width changes from 50 km to 300 km and the ocean depth is 4000

The HKE wave transition on wide shelves is difficult to observe in the global ocean. The circulation pattern of barotropic energy fluxes due to the HKE wave transition, as discussed in Zhang and Yankovsky (2016) and Yankovsky and Zhang (2017), is not observed in the global HYCOM simulations. For most shelves, such as the Queen Charlotte, Amazon, and Sierra Leone shelves, a barotropic energy flux is directed onto the shelf, but a flux circulation pattern with an offshelf barotropic energy flux is not present. The complex shelf bathymetry, insufficiently long or wide shelves, standing waves, and bottom drag may be responsible for this asymmetric flux circulation pattern. We only observe circular energy flux patterns for idealized shelf configurations but not clearly for realistic shelf configurations. Moreover, external factors may make it more challenging to observe HKE wave transitions as seen in idealized model simulations. For example, the HKE wave transition may be affected by offshore standing waves, e.g., Northwest Australia and the Gulf of Alaska, and narrow ocean basins when the width is smaller than the Rossby radius of deformation, e.g., the Equatorial Atlantic Ocean.

Declaration of competing interest

The authors declare that they have no known competing financial interests or personal relationships that could have appeared to influence the work reported in this paper.

Acknowledgments

Harpreet Kaur and Maarten Buijsman are funded by the National Science Foundation (NSF) grant OCE1537449 and National Aeronautics and Space Administration (NASA) grant 80NSSC18K0771. We thank the reviewers for their constructive comments.

Appendix A

In this appendix, we discuss the results for the idealized regional barotropic HYCOM experiments 8 and 9. We include the canyon and the English Channel in experiments 8 and 9, respectively, to understand their effect on the barotropic energy flux patterns of the HKE wave (Figure A.13a and b).

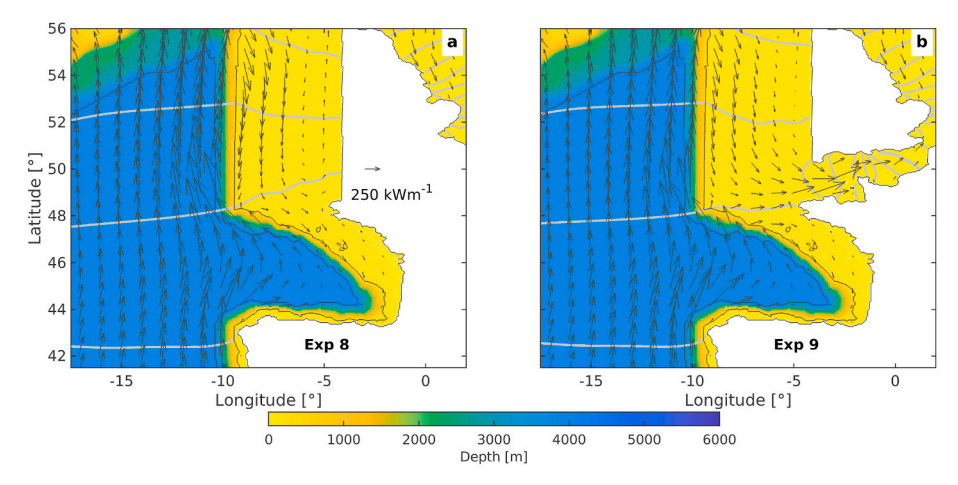


Fig. A.13. The caption is the same as in Fig. 9 but for experiments 8 and 9.

The average onshelf barotropic energy flux along the 250 m isobath at the wide shelf for experiments 8 and 9 is 66 kW m⁻¹ and 82 kW m⁻¹, respectively. Among the three experiments for which Ireland is removed (experiments 7, 8, and 9), the average onshelf barotropic energy flux features a maximum in experiment 7 (126 kW m⁻¹; Table 2) and a minimum in experiment 8 (66 kW m⁻¹). The inclusion of the canyon in experiment 8 reduces the length of the straight shelf, which reduces the integrated onshelf flux. In experiment 9, the English Channel facilitates the onshore propagation of the tidal wave and enhances the onshelf energy flux into the canyon, i.e., it may coincide with and/or mask the onshelf flux due to the HKE wave in the realistic simulation. However, the HKE wave flux pattern is not much affected in both experiments 8 and 9 (Figure A.13a and b).

References

Ansong, J., Arbic, B., Buijsman, M., Richman, J., Shriver, J.F., Wallcraft, A.J., 2015. Indirect evidence for substantial damping of low-mode internal tides in the open ocean. J. Geophys. Res.: Oceans 120. https://doi.org/10.1002/2015JC010998.

Arbic, B.K., Garrett, C., 2010. A coupled oscillator model of shelf and ocean tides. Continent. Shelf Res. 30, 564–574. https://doi.org/10.1016/j.csr.2009.07.008.

Brink, K.H., Chapman, D.C., 1987, second ed.. Programs for Computing Properties of Coastal-Trapped Waves and Wind-Driven Motions over the Continental Shelf and Slope. Woods Hole Oceanographic Institute Tech. Rep. WHOI-87-24, p. 50.

Buijsman, M., Arbic, B., Green, J., Helber, R., Richman, J., Shriver, J., Timko, P., Wallcraft, A., 2015. Optimizing internal wave drag in a forward barotropic model with semidiurnal tides. Ocean Model. 85, 42–55. https://doi.org/10.1016/j. ocemod.2014.11.003.

Buijsman, M.C., Stephenson, G.R., Ansong, J.K., Arbic, B.K., Green, J.M., Richman, J.G., Shriver, J.F., Vic, C., Wallcraft, A.J., Zhao, Z., 2020. On the interplay between horizontal resolution and wave drag and their effect on tidal baroclinic mode waves in realistic global ocean simulations. Ocean Model. 152, 101656 https://doi.org/ 10.1016/j.ocempd.2020.101656.

Clarke, A.J., Battisti, D.S., 1981. The effect of continental shelves on tides. Deep Sea Research Part A. Ocean. Res. Paper. 28, 665–682. https://doi.org/10.1016/0198-0149(81)90128-X.

Dale, A., Huthnance, J., Sherwin, T., 2001. Coastal-trapped waves and tides at near-inertial frequencies. J. Phy. Oceanography. 31, 2958–2970. https://doi.org/10.1175/1520-0485(2001)031<2958:CTWATA>2.0.CO:2.

Egbert, G., Ray, R., 2003. Semi-diurnal and diurnal tidal dissipation from topex-poseidon altimetery. Geophys. Res. Lett. 30 https://doi.org/10.1029/2003GL017676.
Gerkema, T., Zimmerman, J., 2008. An Introduction to Internal Waves. Lecture Notes.

Royal NIOZ, Texel.

Hendershott, M.C., 1972. The effects of solid earth deformation on global ocean tides.

Geophys. J. Int. 29, 389–402. https://doi.org/10.1111/j.1365-246X.1972.tb06167.x.

Huthnance, J.M., 1975. On trapped waves over a continental shelf. J. Fluid Mech. 69,

689–704. https://doi.org/10.1017/S0022112075001632. Huthnance, J.M., 1981. Waves and currents near the continental shelf edge. Prog.

Huthnance, J.M., 1981. Waves and currents near the continental shelf edge. Prog. Oceanogr. 10, 193–226. https://doi.org/10.1016/0079-6611(81)90004-5.

Ivanov, V.A., Shulga, T.Y., Plastun, T., Svishcheva, I.A., 2018. Spatial and temporal parameters of the trapped waves in the black sea shelf areas. Phys. Oceanogr. 25, 280–294. https://doi.org/10.22449/1573-160X-2018-4-280-294.

Jayne, S.R., St Laurent, L.C., 2001. Parameterizing tidal dissipation over rough topography. Geophys. Res. Lett. 28, 811–814. https://doi.org/10.1029/ 2000CL01.2044

Jeon, C.H., Buijsman, M.C., Wallcraft, A.J., Shriver, J.F., Arbic, B.K., Richman, J.G., Hogan, P.J., 2019. Improving surface tidal accuracy through two-way nesting in a global ocean model. Ocean Model. 137, 98–113. https://doi.org/10.1016/jocemod.2019.03.007.

Ke, Z., Yankovsky, A., 2010. The hybrid kelvin-edge wave and its role in tidal dynamics. J. Phys. Oceanogr. 40. 2757–2767. https://doi.org/10.1175/2010JPO4430.1.

Knauss, J.A., Garfield, N., 2016. Introduction to Physical Oceanography, third ed. URL: https://books.google.com/books?id=fp32DQAAOBAJ.

Kunze, E., 2017. The internal-wave-driven meridional overturning circulation. J. Phys. Oceanogr. 47, 2673–2689. https://doi.org/10.1175/JPO-D-16-0142.1.

MacKinnon, J.A., Zhao, Z., Whalen, C.B., Waterhouse, A.F., Trossman, D.S., Sun, O.M., Laurent, L.C.S., Simmons, H.L., Polzin, K., Pinkel, R., Pickering, A., Norton, N.J., Nash, J.D., Musgrave, R., Merchant, L.M., Melet, A.V., Mater, B., Legg, S., Large, W. G., Kunze, E., Klymak, J.M., Jochum, M., Jayne, S.R., Hallberg, R.W., Griffies, S.M., Diggs, S., Danabasoglu, G., Chassignet, E.P., Bujisman, M.C., Bryan, F.O., Briegleb, B. P., Barna, A., Arbic, B.K., Ansong, J.K., Alford, M.H., 2017. Climate process team on internal wave-driven ocean mixing. Bull. Am. Meteorol. Soc. 98, 2429–2454. https://doi.org/10.1175/BAMS-D-16-0030.1.

Munk, W., Snodgrass, F., Wimbush, M., 1970. Tides off-shore: transition from California coastal to deep-sea waters. Geophys. Fluid Dynam. 1, 161–235. https://doi.org/ 10.1080/03091927009365772.

Munk, W., Wunsch, C., 1998. Abyssal recipes ii: energetics of tidal and wind mixing. Deep Sea Res. Oceanogr. Res. Pap. 45, 1977–2010. https://doi.org/10.1016/S0967-0637(98)00070.3

Musgrave, R.C., 2019. Energy fluxes in coastal trapped waves. J. Phys. Oceanogr. 49, 3061–3068. https://doi.org/10.1175/JPO-D-18-0172.1.

Mysak, L.A., 1980. Topographically trapped waves. Annu. Rev. Fluid Mech. 12, 45–76. https://doi.org/10.1146/annurev.fl.12.010180.000401.

Nash, J.D., Alford, M.H., Kunze, E., 2005. Estimating internal wave energy fluxes in the ocean. J. Atmos. Ocean. Technol. 22, 1551–1570. https://doi.org/10.1175/ LTECH1784.1

Schlichting, H., 1968. Boundary Layer Theory. McGraw-Hill, New York.

Waterhouse, A.F., MacKinnon, J.A., Nash, J.D., Alford, M.H., Kunze, E., Simmons, H.L., Polzin, K.L., Laurent, L.C.S., Sun, O.M., Pinkel, R., Talley, L.D., Whalen, C.B., Huussen, T.N., Carter, G.S., Fer, I., Waterman, S., Garabato, A.C.N., Sanford, T.B., Lee, C.M., 2014. Global patterns of diapycnal mixing from measurements of the turbulent dissipation rate. J. Phys. Oceanogr. 44, 1854–1872. https://doi.org/10.1175/JPO-D-13-0104.1.

Yankovsky, A., 2009. Large-scale edge waves generated by hurricane landfall. J. Geophys. Res. 114, C03014 https://doi.org/10.1029/2008JC005113.

Yankovsky, A., Zhang, T., 2017. Scattering of a semidiurnal barotropic kelvin wave into internal waves over wide continental shelves. J. Phys. Oceanogr. 47, 2545–2562. https://doi.org/10.1175/JPO-D-16-0284.1.

Zhang, T., Yankovsky, A., 2016. On the nature of cross-isobath energy fluxes in topographically modified barotropic semidiurnal Kelvin waves. J. Geophys. Res.: Oceans 121, 3058–3074. https://doi.org/10.1002/2015JC011617.